Polymer 79 (2015) 99–109

Contents lists available at ScienceDirect

Polymer

journal homepage: www.elsevier.com/locate/polymer

Cylindrical brush copolymer bearing polystyrene-*block*-poly(ε-caprolactone) diblock side chains: Synthesis *via* a sequential grafting-from polymerization approach and its formation of fibrillar nanophases in epoxy thermosets

Houluo Cong, Lei Li, Sixun Zheng*

Department of Polymer Science and Engineering and the State Key Laboratory of Metal Matrix Composites, Shanghai Jiao Tong University, Shanghai, 200240, PR China

ARTICLE INFO

Article history:
Received 2 June 2015
Received in revised form
23 August 2015
Accepted 5 October 2015
Available online 9 October 2015

Keywords:
Sequential polymerizations with grafting-from methodology
Cylindrical brush copolymer
Block copolymer
Epoxy
Reaction-induced microphase separation
Nanofibers

ABSTRACT

In this contribution, we reported the synthesis of a core-shell cylindrical brush copolymer with poly(2-hydroxyethyl methacrylate) (PHEMA) backbone and polystyrene-*block*-poly(ε-caprolactone) (PS-*b*-PCL) diblock side chains [denoted PHEMA-*g*-(PS-*b*-PCL)$_n$] with the combination of atom transfer radical polymerization, the Huisgen 1,3-dipolar cycloaddition between azido and alkynyl groups and the ring-opening polymerization *via* a sequential "grafting from" polymerization approach. The cylindrical brush block copolymer was characterized by means of ^{1}H nuclear magnetic resonance spectroscopy (NMR), gel permeation chromatography (GPC), atomic force microscopy (AFM) and differential scanning calorimetry (DSC). It is found that the fibrillar nanophases were formed with the length of about 400 nm and the diameter of about 15 nm *via* reaction-induced microphase separation mechanism while this cylindrical block copolymer brush was incorporated into epoxy thermosets. The fibrillar nanophases were characterized by means of transmission electron microscopy (TEM), small-angle X-ray scattering (SAXS) and dynamic mechanical thermal analysis (DMTA). The formation of the fibrillar nanophases was interpreted on the basis of the constraint of cylindrical brush architecture of copolymer on reaction-induced microphase separation behavior.

1. Introduction

Cylindrical brush polymers are a class of high-molecular-weight graft polymers with very dense and regularly spaced side chains along the backbone [1–15]. Owing to the high steric crowding of sides chains, these polymers would display extended macromolecular geometries with cylindrical (or worm-like) conformation and their lengths are up to a few hundred nanometers, which are determined with the polymerization degree of the backbones. Cylindrical brush copolymers can display the features quite different from their linear analogs. Owing to their densely grafted side chains and extended conformation, cylindrical brush copolymers would display low entanglement density. Compared to their linear analogs, the reduced entanglement is prone to forming the nanosized objects with the sizes of the single cylindrical brush copolymers while they are demixed out of solutions [5,14–18]. These structural features have endowed the cylindrical brush copolymers with numerous potential applications in nanoscience, such as nanotubes [5], precursors for nanocapsules [17], molecular actuators [19], templates for inorganic particles [20–22] and other carbon nanostructures [23]. In marked contrast to linear block copolymer analogs, the self-assembly behavior of cylindrical brush copolymers bearing block side chains is constrained by the covalent bonds of the side chains with the backbone chains and thus the morphologies of self-assembly are significantly affected by the limited flexibility of the backbone resulting from the high steric crowding of densely grafted side chains.

Generally, cylindrical brush copolymers can be synthesized with three strategies: i) grafting-through (direct polymerization of macromonomers), ii) grafting-to (coupling of side chains onto the backbone) and iii) grafting-from (polymerization of side chains from the sites in the backbone). The grafting-through method has

* Corresponding author.
E-mail address: szheng@sjtu.edu.cn (S. Zheng).

http://dx.doi.org/10.1016/j.polymer.2015.10.014
0032-3861/

long been used to obtain cylindrical brush copolymers. Nonetheless, it is difficult to control the polymerization degrees of the backbones with conventional radical polymerization. Recently, the control over the length of the backbone has been significantly improved by the use of the macromonomers terminated with norbornene groups *via* ring-opening metathesis polymerization catalyzed with highly active ruthenium catalysts [24–26]. The grafting-to approach is quite dependent on the efficiencies of coupling reaction of the terminal groups of side chains with the backbone. A few high efficient coupling reactions such as copper-catalyzed cycloaddition between azido and alkynyl groups (*i.e.*, click chemistry) have been reported toward this end [27–29]. In the grafting-from approach, the backbone macromolecules are functionalized into the macromolecular initiators or the chain transfer agents, with which controlled/living radical polymerizations [*e.g.*, atom transfer radical polymerization (ATRP), reversible addition–fragmentation chain transfer (RAFT) polymerization] and ring-opening polymerization (ROP) can be carried out to allow the growth of side chains from the initiating sites [30–34]. This approach is very promising to obtain the cylindrical brush copolymers with long backbone and long side chains.

Besides the methodology of synthesis, the studies on the morphologies and self-assembly behavior of cylindrical brush copolymers have also attracted considerable interest of investigators. In ample literature, cylindrical brush copolymers have been reported directly to visualize on the substrates such as silicon wafer and mica by means of scanning electron microscopy (SEM) and atomic force microscopy (AFM) [5,14,33,35–44]. It is found that the morphologies of cylindrical brush copolymers on these inorganic substrates are quite dependent on the interactions of the brushes with the substrates. Matyjaszewski et al. [39] reported that an adsorption-induced backbone scission could occur while all the macromolecules with highly branched architectures including cylindrical brushes were deposited on the inorganic substrates. It is proposed that the attractive interaction between the side chains and the substrate is maximized by the spreading of the side chains, which in turn induces tension along the polymer backbone. Grubbs et al. [45,46] reported the self-assembly behavior of brush block copolymers. Owing to the rigid-rod secondary structure, the self-assembly of these cylindrical block copolymer bushes can rapidly form well-ordered morphologies composed of stacked lamellae with large domain sizes. It was found that the wavelength of reflectance can be synthetically and predictably tuned from the UV to the near IR by manipulation of the polymer chain length. Russell et al. [47,48] investigated the self-assembly behavior of the symmetric cylindrical block copolymers containing approximately equal volume fractions of polystyrene and polylactide brushes. It was found that each symmetric cylindrical block copolymers can be self-assembled into highly ordered lamellae with domain spacing ranging from 20 to 240 nm by varying molecular weight of the backbone in the bulk state as revealed by small-angle X-ray scattering (SAXS). Owing to the reduced degree of chain entanglements of the cylindrical block copolymers, the self-assembly behavior can be utilized rapidly to form two dimensionally well-ordered, periodic nanopatterns on silicon substrate. Although there have been a few previous reports, the self-assembly behavior of cylindrical block copolymer brushes still remained largely unexplored.

In this work, we reported the synthesis of a novel cylindrical brush copolymer bearing diblock side chains. Thereafter, the reaction-induced microphase separation behavior of this cylindrical brush copolymer in epoxy thermosets was investigated. This cylindrical block copolymer is composed of a poly(2-hydroxyethyl methacrylate) (PHEMA) backbone and polystyrene-*block*-poly(ε-caprolactone) (PS-*b*-PCL) diblock side chains [denoted PHEMA-*g*-(PS-*b*-PCL)$_n$]; it would be synthesized with the combination of atom transfer radical polymerization, the Huisgen 1,3-dipolar cycloaddition between azido and alkynyl groups and the ring-opening polymerization *via* a sequential "grafting from" polymerization approach. The cylindrical block copolymer brush is designed and synthesized by knowing that: i) PCL is miscible with epoxy [49,50] after and before curing and ii) PS undergoes a reaction-induced phase separation in the blends with epoxy [51]. Therefore, a reaction-induced microphase separation would occur in the blends of the cylindrical brush copolymer with epoxy. The purpose of this study is to examine the constraint of the cylindrical brush architecture of the diblock copolymer on the reaction-induced microphase separation behavior. In this work, the morphologies of the thermosets were investigated by means of transmission electron microscopy (TEM), small angle X-ray scattering (SAXS) and dynamic mechanical thermal analysis (DMTA).

2. Experimental

2.1. Materials

2-Hydroxyethyl methacrylate (HEMA) was purchased from Aladdin Reagent Co., Shanghai, China. Before use, HEMA was purified by washing with petroleum ether three times. ε-Caprolactone (CL) was purchased from Fluka Co., Germany and it was distilled over CaH_2 under decreased pressure before use. Propargyl alcohol was purchased from Xiya Chemical Reagent Co. China, and distillated before use. Styrene (St) was purchased from Shanghai Reagent Co., China. Before use, St was passed through a basic alumina column to remove the inhibitor. Methyl 2-bromopropionate and *N*,*N*,*N*′,*N*′,*N*″-pentamethyl diethylenetriamine (PMDETA) were purchased from Aldrich Co. USA and used as received. Triethylamine (TEA) was dried over CaH_2 and then treated with *p*-toluenesulfonyl chloride, followed by distillation. Copper (I) bromide (CuBr) and stannous (II) octanoate [Sn(Oct)$_2$] were obtained from Shanghai Reagent Co., China. The epoxy monomer, diglycidyl ether of bisphenol A (DGEBA) was purchased from Shanghai Resin Co., China and it had a quoted epoxide equivalent weight of 185~210. 4,4′-Methylenebis(2-chloroaniline) (MOCA) and 3,5-di-tert-butyl-4-hydroxytoluene were of analytically pure grade, obtained from Shanghai Reagent Co., China. All other reagents were obtained from commercial resources and were purified according to standard procedures prior to use.

2.2. Synthesis of poly(2-hydroxyethyl methacrylate) (PHEMA)

Poly(2-hydroxyethyl methacrylate) (PHEMA) was synthesized *via* the atom transfer radical polymerization (ATRP) of 2-hydroxyethyl methacrylate (HEMA) with methyl 2-bromopropionate as the initiator. Typically, methyl 2-bromopropionate (0.079 g, 0.48 mmol), HEMA (14.403 g, 108.5 mmol), Cu(I)Br (68 mg, 0.48 mmol), PMDETA (90 μL, 0.48 mmol) and anhydrous 1,4-dioxane (15 mL) were added to a pre-dried flask equipped with a magnetic stirrer. The flask was connected to a Schlenk line to degas *via* three pump-freeze-thaw cycles. The polymerization was carried out at 80 °C for 4 h. The crude product was dissolved in methanol and then passed through a neutral alumina column to remove the catalyst. After rotary evaporation, the concentrated solution was dropped into a great amount of cold diethyl ether to afford the precipitates. This procedure was repeated thrice to purify the polymer. After dried in a vacuum oven at 30 °C for 24 h, the polymer (PHEMA) (10.150 g) was obtained with the conversion of HEMA to be *c.a.* 70%. The molecular weight was measured by gel permeation chromatography (GPC) to be $M_n = 20{,}300$ Da with $M_w/M_n = 1.33$. ^{1}H NMR (CD_3OD, ppm): 4.89 [36H, $CH_2O\boldsymbol{H}$], 4.04 [66H, $COOC\boldsymbol{H}_2CH_2OH$], 3.78 [66H,

$COOCH_2C\boldsymbol{H}_2OH$], 3.61 [3H, $C\boldsymbol{H}_3OCOCH(CH_3)$], 2.06–1.92 [51H, $CH_3OCOC\boldsymbol{H}(CH_3)$, $C\boldsymbol{H}_2C(CH_3)$], 1.14–0.88 [87H, $CH_3OCOCH(C\boldsymbol{H}_3)$, $CH_2C(C\boldsymbol{H}_3)$].

2.3. Synthesis of poly(2-(2-bromopropanoyloxy)ethyl methacrylate) (PBPEMA)

Poly(2-(2-bromopropanoyloxy)ethyl methacrylate) (PBPEMA) was synthesized *via* the reaction of poly(2-hydroxyethyl methacrylate) (PHEMA) with 2-bromopropionyl bromide. Typically, PHEMA (3.061 g, 23.5 mmol with respect of 2-hydroxyethyl groups), triethylamine (TEA) (2.372 g, 23.5 mmol) and 15 mL of anhydrous N,N-dimethylformamide (DMF) were added into a flask with vigorous stirring and then 2-bromopropionyl bromide (6.091 g, 28.2 mmol) was dropwise added at 0 °C within 30 min. The reaction was performed at room temperature for 24 h and the reacted mixture was dropped into deionized water to afford the precipitates. The precipitates was dissolved with dichloromethane (30 mL) and the solution was washed with the aqueous solution of $NaHCO_3$ (0.50 M, 15 mL) and deionized water (15 mL × 3). Thereafter, anhydrous Na_2SO_4 was added to dry the solution. The dried solution was concentrated *via* rotary evaporation and the concentrated solution was dropped into methanol to obtain the precipitates. After dried in a vacuum oven at 30 °C for 24 h, the product (5.570 g) was obtained with the yield of *c.a.* 49%. ^{1}H NMR ($CDCl_3$, ppm): 4.52~4.31 [41H, -$COOC\boldsymbol{H}_2C\boldsymbol{H}_2OOC$-], 4.25~4.10 [20H, -$C\boldsymbol{H}(Br)CH_3$], 3.72 [1H, $CH_3OCOC\boldsymbol{H}(CH_3)$], 3.55 [2H, $C\boldsymbol{H}_3OCOCH(CH_3)$], 1.86 [3H, $C\boldsymbol{H}_2C(CH_3)$], 1.93 [51H, $CH_2{=}CC\boldsymbol{H}_3$], 1.14~0.88 [35H, CH_3OC-$OCH(C\boldsymbol{H}_3)$, $CH_2C(C\boldsymbol{H}_3)$, CH(Br)$C\boldsymbol{H}_3$].

2.4. Synthesis of PHEMA-g-(PS-Br)$_n$

Typically, the above PBPEMA [98 mg, 0.24 mmol with respect of 2-(2-bromopropanoyloxy)ethyl groups], St (16.364 g, 154 mmol), Cu(I)Br (34 mg, 0.24 mmol), PMDETA (48 μL, 0.24 mmol) and anhydrous toluene (40 mL) were added to a flask equipped with a magnetic stirrer. The flask was connected to the Schlenk line to degas *via* three pump-freeze-thaw cycles. The polymerization was carried out at 65 °C for 20 h and then 20 mL of tetrahydrofuran was added to the reacted mixture. The solution was passed through a neutral alumina column to remove the catalyst. The as-obtained solution was concentrated *via* rotary evaporation and the concentrated solution was dropped into a great amount of cold methanol to afford the precipitates. The precipitates were re-dissolved with tetrahydrofuran and the solution was re-dropped into cold methanol; this procedure was repeated thrice to purify the polymer. After dried in a vacuum oven at 30 °C for 24 h, the polymer [denoted PHEMA-*g*-(PS-Br)$_n$] (1.68 g) was obtained with the conversion of St to be *c.a.* 10%. ^{1}H NMR ($CDCl_3$, ppm): 7.29~6.31 [72H, $CH_2CH(C_6\boldsymbol{H}_5)$], 4.61~4.38 [2H, $COOC\boldsymbol{H}_2C\boldsymbol{H}_2OOC$, $C\boldsymbol{H}$(Br)C_6H_5], 3.78~3.45 [1H, $C\boldsymbol{H}_3OCOCH(CH_3)$, $CH_3OCOC\boldsymbol{H}(CH_3)$], 1.89~1.83 [16H, $C\boldsymbol{H}_2C(CH_3)$, $CH_2C\boldsymbol{H}(C_6H_5)$], 1.63~1.33 [27H, $OCOC\boldsymbol{H}(CH_3)$, $C\boldsymbol{H}_2CH(C_6H_5)$], 0.98~0.68 [2H, $CH_3OCOCH(C\boldsymbol{H}_3)$, $CH_2C(C\boldsymbol{H}_3)$, CH(Br)$C\boldsymbol{H}_3$]. The molecular weight was measured by gel permeation chromatography (GPC) to be M_n = 452,400Da with M_w/M_n = 1.50.

2.5. Synthesis of PHEMA-g-(PS-b-PCL)$_n$

First, PHEMA-*g*-(PS-N_3)$_n$ was prepared *via* the reaction of PHEMA-*g*-(PS-Br)n with sodium azide (NaN_3). Typically, the PHEMA-*g*-(PS-Br)$_n$ (1.571 g), NaN_3 (0.28 g, 4.3 mmol) and anhydrous DMF (20 mL) were added to a flask equipped with a magnetic stirrer. The reaction was carried out at room temperature for 24 h. The reacted mixture was dropwise added to 200 mL of the mixture of water with methanol (v/v = 1/1) to obtain the precipitates. The procedure was repeated three times. After drying *in vacuo* at 30 °C for 24 h, the product [denoted PHEMA-*g*-(PS-N_3)$_n$] (1.492 g) was obtained with the yield of *c.a.* 95%. ^{1}H NMR ($CDCl_3$, ppm): 7.29~6.31 [104H, $CH_2CH(C_6\boldsymbol{H}_5)$], 4.00~3.45 [1H, $COOC\boldsymbol{H}_2C\boldsymbol{H}_2OOC$, $C\boldsymbol{H}$(Br)C_6H_5], 1.89~1.83 [24H, $C\boldsymbol{H}_2C(CH_3)$, $CH_2C\boldsymbol{H}(C_6H_5)$], 1.63~1.33 [42H, $OCOC\boldsymbol{H}(CH_3)$, $C\boldsymbol{H}_2CH(C_6H_5)$], 0.98~0.68 [3H, $CH_3OCOCH(C\boldsymbol{H}_3)$, $CH_2C(C\boldsymbol{H}_3)$, CH(Br)$C\boldsymbol{H}_3$].

Second, the copper-catalyzed cycloaddition between PHEMA-*g*-(PS-N_3)$_n$ and propargyl alcohol was carried out to afford a PHEMA-*g*-(PS-OH)$_n$. Typically, to a flask equipped with a magnetic stirrer, PHEMA-*g*-(PS-N_3)$_n$ (1.411 g), propargyl alcohol (0.363 g, 6.5 mmol), Cu(I)Br (17 mg, 0.12 mmol), PMDETA (24 μL, 0.12 mmol) and anhydrous DMF (20 mL) were charged with vigorous stirring. The flask was connected to a Schlenk line to degas *via* three pump-freeze-thaw cycles. Thereafter, the reaction was carried out at 30 °C for 36 h. The crude product was dissolved in tetrahydrofuran and then passed through a neutral alumina column to remove the catalyst. The mixture was concentrated *via* rotary evaporation and then concentrated solution was precipitated in a great amount of cold methanol. The procedure of dissolving and precipitation was repeated three times to purify the product. After dried in a vacuum oven at 30 °C for 24 h, the product [denoted PHEMA-*g*-(PS-OH)$_n$] (1.190 g) was obtained with the yield of *c.a.* 84%. ^{1}H NMR ($CDCl_3$, ppm): 7.29~6.31 [399H, $CH_2CH(C_6\boldsymbol{H}_5)$], 5.11 [1H, $C\boldsymbol{H}(C_6H_5)$N], 4.69 [2H, $C\boldsymbol{H}_2OH$], 3.90~3.45 [4H, $COOC\boldsymbol{H}_2C\boldsymbol{H}_2OOC$], 1.89~1.83 [86H, $C\boldsymbol{H}_2C(CH_3)$, $CH_2C\boldsymbol{H}(C_6H_5)$], 1.63~1.33 [146H, $OCOC\boldsymbol{H}(CH_3)$, $C\boldsymbol{H}_2CH(C_6H_5)$], 0.98~0.68 [9H, $CH_3OCOCH(C\boldsymbol{H}_3)$, $CH_2C(C\boldsymbol{H}_3)$, CH(Br)$C\boldsymbol{H}_3$].

Third, the cylindrical brush copolymer bearing PS-*b*-PCL diblock copolymer side chains [denoted PHEMA-*g*-(PS-*b*-PCL)$_n$] was synthesized *via* the ring opening polymerization (ROP) of ε-caprolactone (ε-CL) with the above PHEMA-*g*-(PS-OH)$_n$ as the macromolecular initiator. Typically, PHEMA-*g*-(PS-OH)$_n$ (0.752 g, 0.96 mmol with the respect of hydroxyl groups), ε-CL (1.050 g, 9.2 mmol) and anhydrous toluene (1.5 mL) were added to a pre-dried flask equipped with a magnetic stirrer. The flask was connected to the Schlenk line and the system was degassed *via* three pump-freeze-thaw cycles. With $Sn(Oct)_2$ (2.0 mg) dissolved in anhydrous toluene as the catalyst, the ring-opening polymerization of CL was carried out at 120 °C for 24 h. Cooled to room temperature, the crude product was dissolved in dichloromethane (20 mL) and the solution was dropped into 100 mL of cold methanol to afford the precipitates. The procedure of dissolution and precipitation was repeated three times to purify the polymer. After dried in a vacuum oven at 30 °C for 24 h, the product (1.660 g) was obtained with the yield of *c.a.* 87%. ^{1}H NMR ($CDCl_3$, ppm): 7.29~6.31 [144H, $CH_2CH(C_6\boldsymbol{H}_5)$], 5.11~5.01 [3H, -$C\boldsymbol{H}(C_6H_5)$N, CH=C(N)$C\boldsymbol{H}_2$O-], 4.05 [40H, $OCO(CH_2)_4C\boldsymbol{H}_2$], 3.65 [1H, $CH_2C\boldsymbol{H}_2OH$], 2.30 [42H, $OCOC\boldsymbol{H}_2(CH_2)_4$], 2.12~1.73 [34H, $C\boldsymbol{H}_2C(CH_3)$, $CH_2C\boldsymbol{H}(C_6H_5)$], 1.64 [106H, $OCOCH_2C\boldsymbol{H}_2CH_2C\boldsymbol{H}_2CH_2$], 1.54~1.33 [90H, $OCOC\boldsymbol{H}(CH_3)$, $C\boldsymbol{H}_2CH(C_6H_5)$, $OCOCH_2CH_2C\boldsymbol{H}_2CH_2CH_2$], 0.98~0.68 [4H, CH_3OC-$OCH(C\boldsymbol{H}_3)$, $CH_2C(C\boldsymbol{H}_3)$, CH(Br)$C\boldsymbol{H}_3$]. According to end group analysis with ^{1}H NMR spectroscopy, the length of PCL block in the brush copolymer was determined to be L_{PCL} = 3200 Da. Therefore, the molecular weight was calculated to be M_n = 1,022,000 Da.

2.6. Preparation of epoxy thermosets

Desired amount of PHEMA-*g*-(PS-*b*-PCL)$_n$ was added to the mixture of DGEBA and dichloromethane with vigorous stirring until a full dissolution was attained. The solvent was evaporated at 80 °C and then the curing agent (viz. MOCA) was added with vigorous stirring until a full dissolution of the curing agent. The ternary mixture was poured into Teflon molds to cure at 150 °C for 3 h plus 180 °C for 2 h.

2.7. Measurements and characterization

2.7.1. Nuclear magnetic resonance (NMR) spectroscopy

The NMR spectroscopy was carried out on a Varian Mercury Plus 400 MHz NMR spectrometer at 25 °C. Deuterium methanol (CD_3OD) or deuterium chloroform ($CDCl_3$) was used to dissolve the samples and the NMR spectra were obtained with tetramethylsilane (TMS) as an internal reference.

2.7.2. Gel permeation chromatography (GPC)

The GPC measurements were carried out a Waters 1515 gel permeation chromatography system equipped with three Waters HR columns (HR4, HR3 and HR1). This apparatus was composed of an Isocratic HPLC pump and a RI detector. The measurements were carried out with N,N′-dimethylformamide (DMF) containing 0.01 M LiBr as an eluent at the flow rate of 1.0 mL/min. The molecular weights and molecular weight distribution were also measured on a Waters 2489 gel permeation chromatography apparatus equipped with Waters RH columns. This apparatus was equipped with a DAWN HELEOS-II multiangle laser light scattering detector; the measurements were carried out at 25 °C with DMF as the eluent at the rate of 1.0 mL/min. The values of all the molecular weights were given on the basis of the measurement of the GPC apparatus equipped with multiangle laser light scattering detector.

2.7.3. Differential scanning calorimetry (DSC)

The DSC measurements were carried out on a TA Instruments Q2000 differential scanning calorimeter in a dry nitrogen atmosphere. The instrument was calibrated with a standard indium. The samples (about 10.0 mg) were first heated up to 180 °C and held at this temperature for 3 min to eliminate thermal history, followed by quenching to −80 °C. In all the cases, a heating rate of 20 °C/min was used to record the heating thermograms and the cooling rate of −10 °C/min to record the cooling thermograms. Glass transition temperatures (T_g) were taken as the midpoint of heat capacity change; melting and crystallization temperatures (T_m) were taken as the temperatures at the maxima of endothermic transitions and the minima of exothermic transitions, respectively.

2.7.4. Dynamic mechanical thermal analysis (DMTA)

The DMTA measurements were carried out on a TA Instruments DMA Q800 dynamic mechanical thermal analyzer equipped with a liquid nitrogen apparatus in a single cantilever mode. The frequency used is 1.0 Hz and the heating rate 3.0 °C/min. The specimen dimension was 1.2 × 2 × 0.1 cm^3. The measurements were performed from −80 °C until the specimens became too soft to be tested.

2.7.5. Atomic force microscopy (AFM)

For the morphological observation of the samples in bulks, the solutions of cylindrical brush copolymers at the concentration of 10 wt% were cast on to glass slides and the films with the thickness of about 25 μm were obtained after the solvent was eliminated at room temperature *in vacuo* for 24 h. Prior to the morphological observation, the specimens were annealed at 80 °C for 30 min and cooled to room temperature. The AFM experiments were performed with a CSPM5500 scanning probe microscope (Benyuan Nano-instruments Ltd, Beijing, China). Tapping mode was employed in air using a tip fabricated from silicon (125 μm in length with *c.a.* 300 kHz resonant frequency). A scan speed during recording was 10 line × s^{-1} using scan heads with a maximum range of 13 × 13 μm.

2.7.6. Transmission electronic microscopy (TEM)

Morphological observation was conducted on a JEOL JEM 2100F transmission electron microscope at a voltage of 120 kV. The thermosets were trimmed using an ultrathin microtome machine and the section specimens with the thickness of 70 nm were placed in 200 mesh copper grids. Before observation, the samples were stained with OsO_4 to increase the contrast.

2.7.7. Small-angle X-ray scattering (SAXS)

The SAXS measurements were performed on a small-angle X-ray scattering beamline of Shanghai Synchrotron Radiation Facility (SSRF), China. Two-dimensional diffraction patterns were recorded using an image intensified CCD detector. The experiments were carried out at room temperature (25 °C) under condition of 8 keV photon energy and 300 nm small-angle resolutions. For the measurements at elevated temperatures, a TH MS600 Linkam hot stage with the precision of 0.1 °C was used as an insertion device. Two dimensional diffraction patterns were recorded by using an image intensified CCD detector. The intensity profiles were output as the plot of scattering intensity (I) *versus* scattering vector, $q = (4\pi/\lambda)\sin(\theta/2)$ (θ = scattering angle).

3. Results and discussion

3.1. Synthesis and characterization of PHEMA-g-(PS-b-PCL)$_n$ brush copolymer

The route of synthesis for the cylindrical brush copolymer with poly(2-hydroxyethyl methacrylate) (PHEMA) backbone and with polystyrene-*block*-poly(ε-caprolactone) (PS-*b*-PCL) diblock copolymers side chains is shown in Scheme 1. The tandem polymerizations with "grafting through" methodology were utilized to obtain the cylindrical brush copolymer bearing diblock side chains. First, poly(2-hydroxyethyl methacrylate) (PHEMA) was synthesized *via* the atom transfer radical polymerization (ATRP) of 2-hydroxyethyl methacrylate (HEMA) with methyl 2-bromopropionate as the initiator. Second, the as-polymerized PHEMA was used to react with 2-bromopropionyl bromide to afford poly(2-(2-bromopropanoyloxy)ethyl methacrylate) (PBPEMA). Third, the PBPEMA was used as the macromolecular initiator to obtain a PS-grafted PHEMA [denoted PHEMA-*g*-(PS-Br)$_n$] *via* the atomic transfer radical polymerization (ATRP) of styrene. Fourth, the terminal bromine atoms of the PS side chains of PHEMA-*g*-(PS-Br)$_n$ were substituted with azido groups *via* the reaction of PHEMA-*g*-(PS-Br)$_n$ with sodium azide (NaN_3), *i.e.*, PHEMA-*g*-(PS-N_3)$_n$ was obtained. Thereafter, the Huisgen 1,3-dipolar cycloaddition between the PHEMA-*g*-(PS-N_3)$_n$ and propargyl alcohol was carried out to obtain the PHEMA-*g*-(PS-OH)$_n$. Finally, the brush copolymer PHEMA-*g*-(PS-OH)$_n$ was employed as a macromolecular initiator to initiate the ring-opening polymerization of ε-caprolactone (CL) to obtain the cylindrical brush copolymer [denoted PHEMA-*g*-(PS-*b*-PCL)$_n$]. Shown in Fig. 1 are the ^{1}H NMR spectra of PHEMA, PBPEMA and the PHEMA-*g*-(PS-Br)$_n$. For PHEMA, the signals of resonance at 3.78 and 4.83 ppm were assignable to the protons of methylene groups in hydroxyethyl groups. After the reaction of the PHEMA with 2-bromopropionyl bromide, the resonance of hydroxyl proton at 4.83 ppm completely disappeared. In the meantime, the signal of resonance for the methylene protons at 3.78 ppm totally shifted to 4.38 ppm. Concurrently, the peak of resonance at 4.40 ppm assignable to the methylene protons connected to methacrylic moiety of PHEMA also completely shifted to 4.48 ppm. This observation indicates that the reaction of PHEMA with 2-bromopropionyl bromide was performed to completion, *i.e.*, PBPEMA was successfully obtained. With the PBPEMA as the macromolecular initiator, the atom transfer radical polymerization of styrene was carried out with the mixture of Cu(I)Br with PMDETA as the catalyst and the PHEMA-*g*-(PS-Br)$_n$

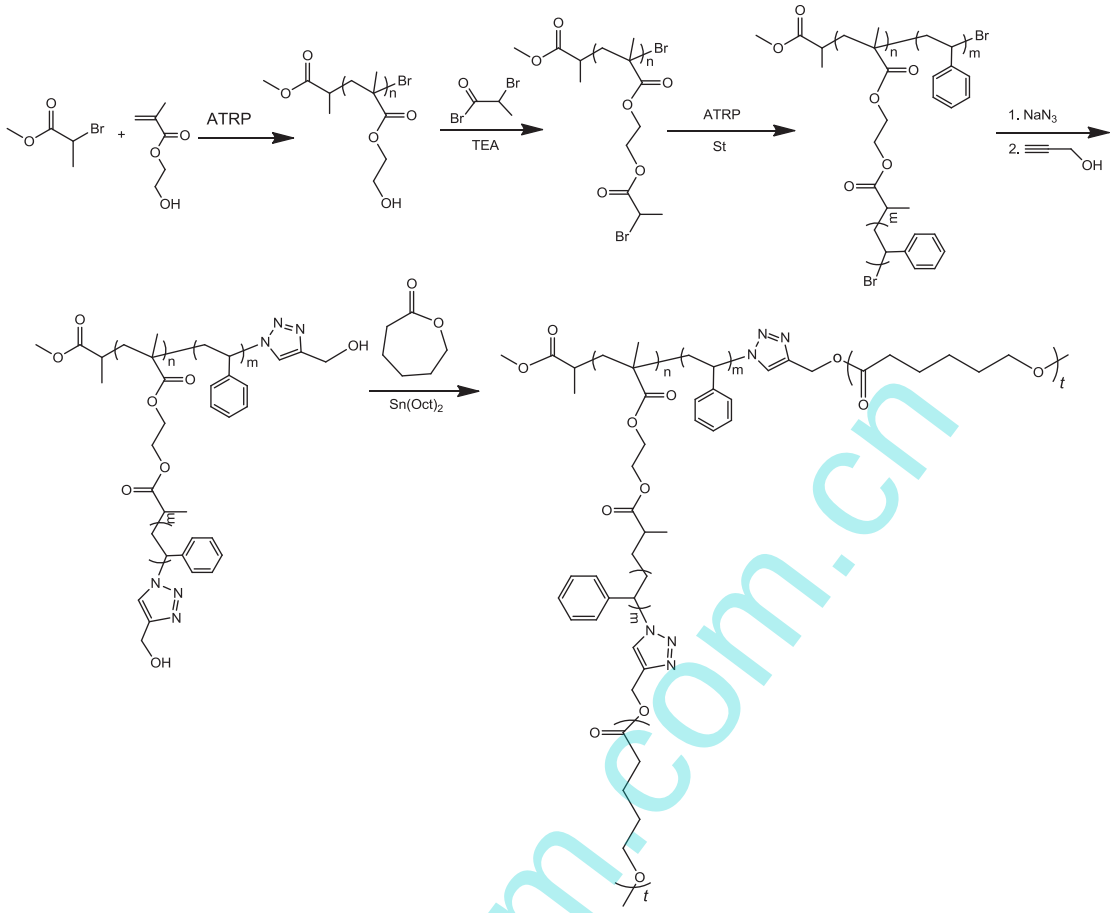

Scheme 1. The route of synthesis of the PHEMA-*g*-(PS-*b*-PCL) copolymer.

brush copolymer was obtained. For PHEMA-*g*-(PS-Br)$_n$ brush copolymer, the signals of resonance at 7.29~6.31 ppm were assignable to the protons of aromatic rings in PS side chains whereas the resonance of protons of methylene and methine in the PS main chains were detected at 1.89~1.83 and 1.63~1.33 ppm, respectively. In addition, the signals of resonance characteristic of the backbone (*viz*. PHEMA) were discernable at 0.72 and 4.43 ppm. The ^{1}H NMR spectroscopy indicates that the PHEMA-*g*-(PS-Br)$_n$ brush copolymer was successfully obtained.

With the reaction of PHEMA-*g*-(PS-Br)$_n$ with sodium azide (NaN_3), the terminal bromine atoms at the PS side chain ends would be substituted with azido groups. This reaction was evidenced by the observation that the signal of resonance at 4.43 ppm assignable to the proton of methine at the ends of PS side chains of PHEMA-*g*-(PS-Br)$_n$ (See Fig. 1) totally shifted to 3.98 ppm (See Fig. 2). In other words, the PHEMA-*g*-(PS-Br)$_n$ has been successfully transformed into PHEMA-*g*-(PS-N_3)$_n$, *i.e.*, the end groups of PS subchains were fully capped with azido groups. With the Huisgen 1,3-dipolar cycloaddition between the PHEMA-*g*-(PS-N_3)$_n$ and propargyl alcohol, notably, the resonance of the methine proton at the ends of PS subchains of PHEMA-*g*-(PS-N_3)$_n$ completely shifted to 5.11 ppm. In the meantime, there appeared a signal of resonance at 4.69 pm, assignable to the protons of methylene in the terminal hydroxymethyl groups connected to triazole ring resulting from the "click" reaction. The ^{1}H NMR spectroscopy indicates that PHEMA-*g*-(PS-OH)$_n$ brush copolymer was obtained. The PHEMA-*g*-(PS-OH)$_n$ brush copolymer was used as the macromolecular initiator for the ring-opening polymerization of ε-caprolactone (CL) to afford the PHEMA-*g*-(PS-*b*-PCL)$_n$ brush copolymer. The ^{1}H NMR spectrum of PHEMA-*g*-(PS-*b*-PCL)$_n$ was presented in Fig. 2. The signals of resonance at 1.38 and 1.84 ppm were assignable to the protons of methylene and methine groups in PS main chains whereas the resonance at the range of 7.29~6.31 ppm were attributable to the protons of aromatic rings of PS subchains. In addition, the signals of proton resonance assignable to PCL chains were clearly exhibited. The peaks of resonance at 1.38, 1.65, 2.30 and 4.05 ppm are assignable to the protons of methylene groups of PCL subchains as indicated in this spectrum. It should be pointed out that the signal of resonance at 3.65 ppm is assignable to the methylene protons of hydroxymethyl groups (*i.e.*, -C***H***$_2$OH) at the terminal ends of PCL chains. According to the ratio of the integral intensity of this peak to those of methylene protons in the middle of PCL main chains, the length of the PCL blocks was estimated to be $L_{PCL} = 3200$ Da. The ^{1}H NMR spectroscopy showed that the resulting brush copolymer combined the structural features from PS and PCL blocks. To measure the molecular weights, the above PHEMA, PHEMA-*g*-(PS-Br)$_n$ and PHEMA-*g*-(PS-*b*-PCL)$_n$ were subjected to gel permeation chromatography (GPC) and the GPC curves were shown in Fig. 3. In all the cases, the GPC curves displayed unimodal peaks. For PHEMA, the molecular weight was measured to be $M_n = 20{,}300$Da with $M_w/M_n = 1.33$ and the degree of polymerization (DP) was thus calculated to be 178. For PHEMA-*g*-(PS-Br)$_n$, the molecular weight was measured to be $M_n = 452{,}400$Da with $M_w/M_n = 1.50$, with which the length of PS blocks in the side chains was estimated to be $L_{PS} \approx 2600$ Da, assuming that each 2-bromopropionyl group in PBPEMA acted as an effective initiating site for a PS side chain. For PHEMA-*g*-(PS-*b*-PCL)$_n$, the length of PCL blocks was estimated to be $L_{PCL} = 3{,}200$Da. Therefore, the molecular weight of the PHEMA-*g*-

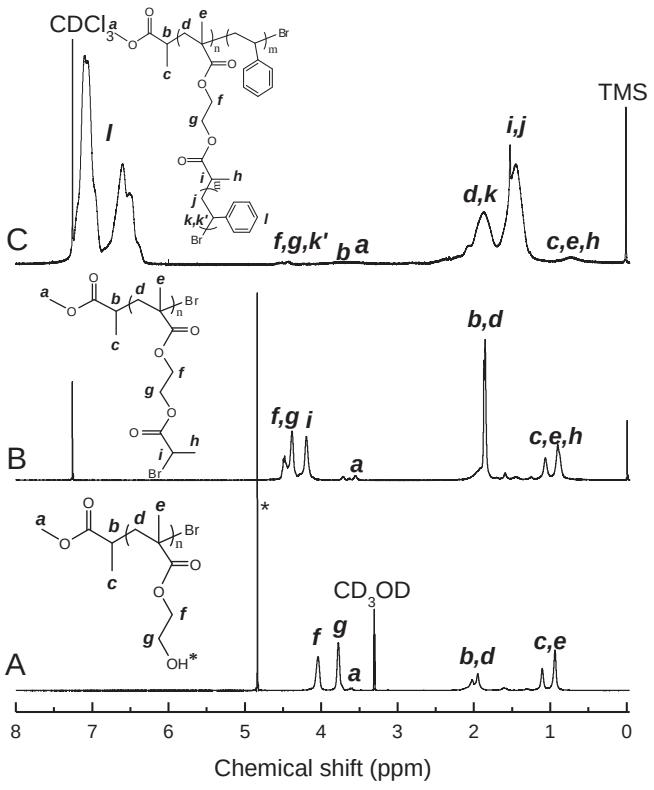

Fig. 1. ^{1}H NMR spectra of: (A) PHEMA; (B) PBPEMA and (C) PHEMA-*g*-(PS-Br)$_n$.

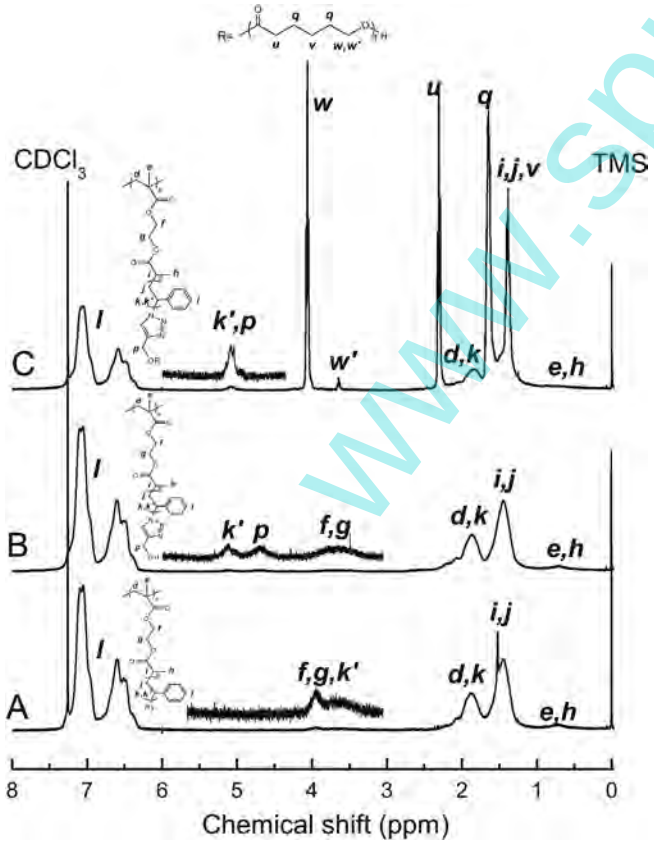

Fig. 2. ^{1}H NMR spectra of: (A) PHEMA-*g*-(PS-N_3)$_n$; (B) PHEMA-*g*-(PS-OH)$_n$ and (C): PHEMA-*g*-(PS-*b*-PCL)$_n$.

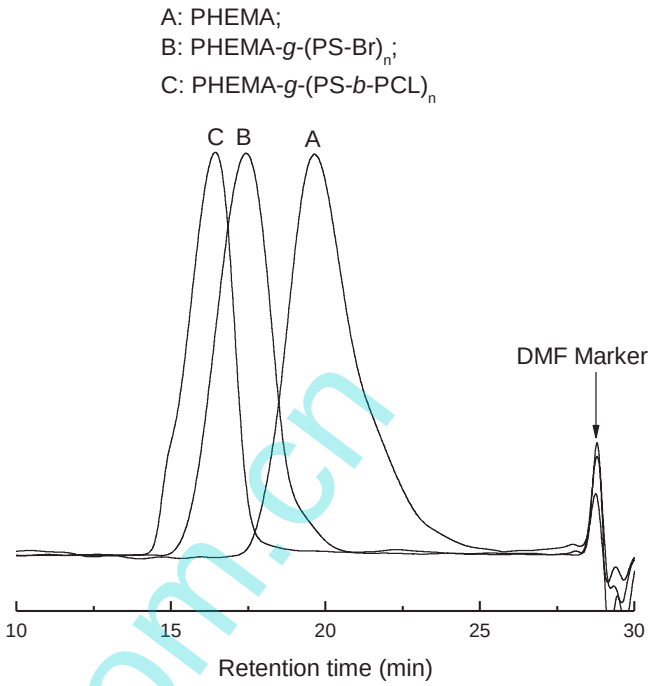

Fig. 3. GPC curves of: (A) PBPEMA; (B) PHEMA-*g*-(PS-Br)$_n$ and (C) PHEMA-*g*-(PS-*b*-PCL)$_n$.

(PS-*b*-PCL)$_n$ copolymer was calculated to be M_n = 1,022,000 Da. The results of ^{1}H NMR and GPC indicate that the cylindrical brush copolymer PHEMA-*g*-(PS-*b*-PCL)$_n$ was successfully obtained. According to the results of GPC and ^{1}H NMR spectroscopy, an extended PHEMA-*g*-(PS-*b*-PCL)$_n$ brush was estimated to have the size as shown in Scheme 2.

To investigate the microphase-separated behavior of the cylindrical brush copolymer in bulks, the PHEMA-*g*-(PS-*b*-PCL)$_n$ was subjected to differential scanning calorimetry (DSC) and both the heating and cooling DSC curves are shown in Fig. 4. In the heating DSC curve, a glass transition at T_g = 95 °C and an endothermic peak at 53 °C were exhibited. The former is attributable to PS subchains whereas the latter to the melting transition of PCL subchains. The fact that the melting peak of PCL subchain (at 53 °C) appeared ahead of the glass transition of PS block (at 95 °C) indicates that the cylindrical brush copolymer bearing PS-*b*-PCL diblock side chains was microphase-separated. Owing to the microphase separation behavior, the PCL subchains in the cylindrical brush copolymer still remained crystallizable while the cylindrical brush copolymer was cooled from the melt. Also shown in Fig. 4 is the cooling DSC curve; the crystallization of PCL subchains occurred at 18 °C. The microphase-separated behavior was further confirmed by atomic force microscopy (AFM). Shown in Fig. 5 are the AFM micrograph of the PHEMA-*g*-(PS-*b*-PCL)$_n$ brush copolymer in bulks. In term of the difference in viscoelasticity between PS and PCL blocks, the dark regions are attributable to PCL microdomains and the light to PS. The AFM result indicates that the cylindrical brush copolymer was indeed microphase-separated.

3.2. Reaction-induced microphase separation behavior

3.2.1. Transmission electron microscopy (TEM)

The above cylindrical brush copolymer was incorporated into epoxy to obtain the thermosets containing PHEMA-*g*-(PS-*b*-PCL)$_n$ copolymer. All the ternary mixtures composed of DGEBA, MOCA

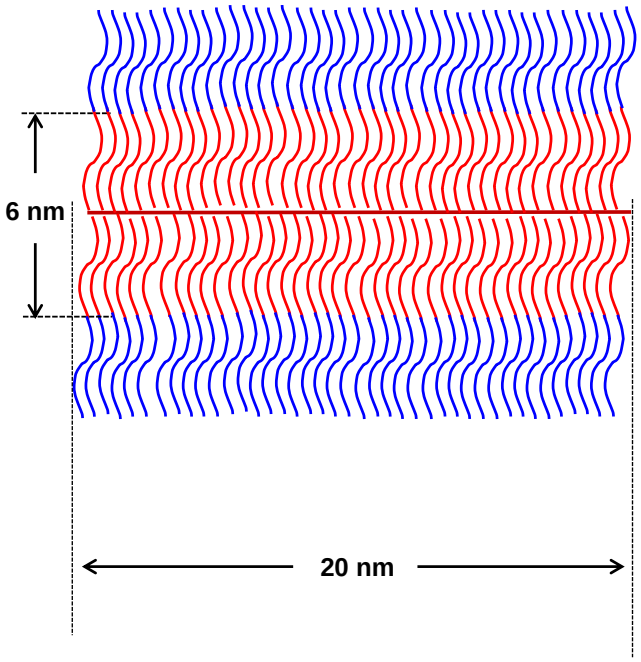

Scheme 2. Size of a PHEMA-*g*-(PS-*b*-PCL)$_n$ bush copolymer.

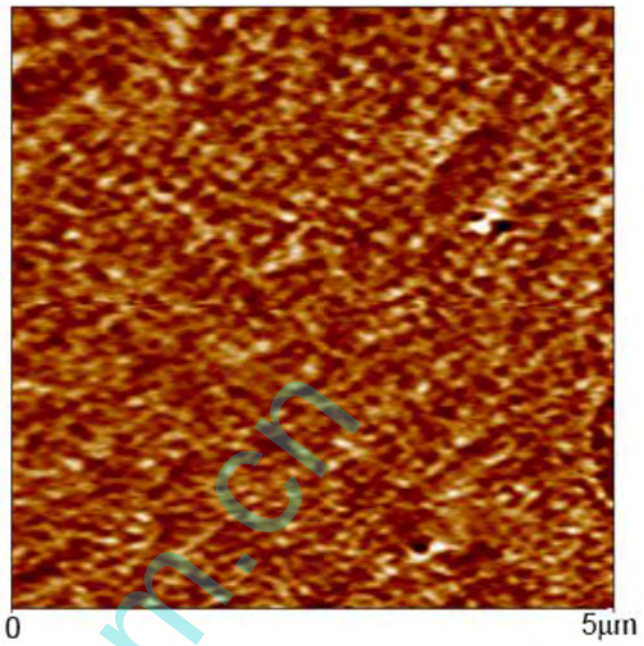

Fig. 5. AFM images of PHEMA-*g*-(PS-*b*-PCL)$_n$ brush copolymer films casting onto silica wafer from 10 wt% of dichloromethane solution.

and PHEMA-*g*-(PS-*b*-PCL)$_n$ were homogenous and transparent at room temperature and 150 °C, suggesting that no macroscopic phase separation occurred. The mixtures were cured at 150 °C for 3 h to obtain the thermosets. In this work, the epoxy thermosets were obtained with the content of PHEMA-*g*-(PS-*b*-PCL)$_n$ up to 40 wt%. All the thermosets were homogenous and transparent, suggesting that there was no macroscopic phase separation at the scale exceeding the wavelength of visible light. The morphologies of the thermosets were investigated by means of transmission electron microscopy (TEM) and the TEM micrographs of the thermosets containing 10, 20, 30 and 40 wt% of PHEMA-*g*-(PS-*b*-PCL)$_n$ are shown in Fig. 6. To increase the contrast, the specimens were stained with OsO_4. In this case, the epoxy matrix was stained whereas the microdomains of PS (if any) remained less affected. The thermoset containing 10 wt% of PHEMA-*g*-(PS-*b*-PCL)$_n$ displayed some nanofiber-like features, which were dispersed into the continuous matrix (See Fig. 6A). A single nanofiber had the size of about 400 nm in length and 15 nm in the diameter of the cross section. With increasing the content of PHEMA-*g*-(PS-*b*-PCL)$_n$, the number of the fibrillar nanodomains increased whereas their sizes remained almost unchanged (See Fig. 6B through D). It is judged that the fibrillar nanophases were attributable to the PS and the continuous matrix to epoxy network that remained mixed with PCL blocks. Notably, the average contour length of a single fibrillar nanodomain was almost twenty times as the length of a single extended cylindrical brush which was estimated according to the polymerization degrees of PHEMA backbone (about 20 nm). The width of each single nanofiber (*viz. c.a.*, 15 nm) was also three times as the diameter of the core of the core–shell cylindrical brush according to the degree of polymerization ($DP_{PS} \approx 28$) of the PS subchains (assuming that the PS subchains were fully extended). According to the size of the fibrillar nanophases revealed in Fig. 6, it is judged that the fibrillar nanodomains observed in the TEM images were the aggregates of a few single cylindrical copolymer brushes, most of which jointed end to end (See Scheme 3). More importantly, the aggregation occurred along the direction of the backbone of the cylindrical brush copolymer.

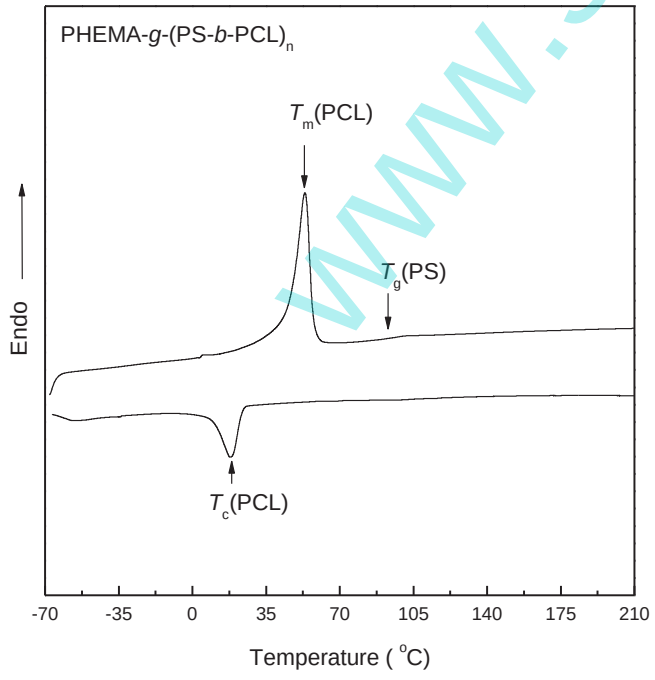

Fig. 4. DSC curves of PHEMA-*g*-(PS-*b*-PCL)$_n$ brush copolymer. Up: heating scanning at 20 °C/min; down: cooling scanning at −10 °C/min.

3.2.2. *Small-angle X-ray scattering*

The morphologies of the thermosets containing PHEMA-*g*-(PS-*b*-PCL)$_n$ was further investigated by means of small angle X-ray scattering (SAXS). Shown in Fig. 7 are the SAXS profiles of the epoxy thermosets containing 10, 20, 30 and 40 wt% of PHEMA-*g*-(PS-*b*-PCL)$_n$. In all the cases, the scattering phenomena were exhibited; the scattering intensity increased with increasing the content of PHEMA-*g*-(PS-*b*-PCL)$_n$. The SAXS results indicate that the epoxy

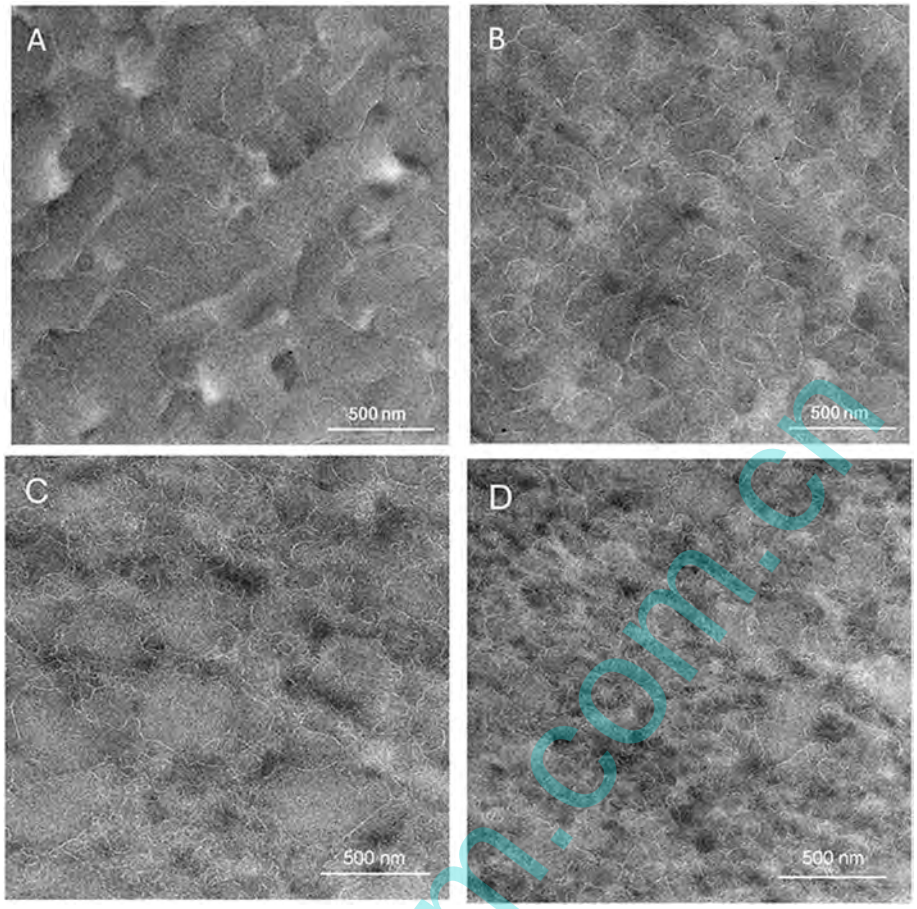

Fig. 6. TEM images of the thermosets containing: A) 10, B) 20, C) 30 and D) 40 wt% of PHEMA-*g*-(PS-*b*-PCL)$_n$ brush copolymer.

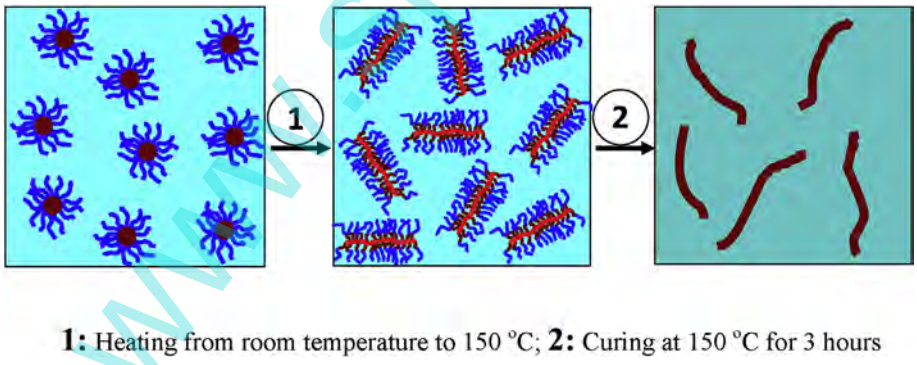

Scheme 3. Formation of fibrillar PS nanophase in epoxy thermoset.

thermosets containing PHEMA-*g*-(PS-*b*-PCL)$_n$ were indeed inhomogeneous at the nanometer scale. The inhomogeneity could be associated with the formation of the fibrillar nanophases of PS, *i.e.*, the thermosets were microphase-separated. It is of interest to note that the form factor scattering from the fibrillar PS microdomains was quite different from those of spherical, cylindrical and lamellar microdomains from the self-assembly which are based on the aggregation of the blocks of different block copolymers.

3.2.3. Dynamic mechanical thermal analysis (DMTA)

The above epoxy thermosets containing PHEMA-*g*-(PS-*b*-PCL)$_n$ cylindrical brush copolymer were subjected to dynamic mechanical thermal analysis (DMTA) and the DMTA spectra are shown in Fig. 8. For the control epoxy, a major transition (*viz.* α-transition) was exhibited at *c.a.* 159 °C and it was responsible for the glass–rubber transition of the crosslinked polymer. Apart from the α-transition, the crosslinked network exhibited the secondary transitions (*viz.* β-transition) at approximately −56 and 73 °C, respectively. The former is attributed predominantly to the motion of hydroxyl ether structural units [-$CH_2CH(OH)CH_2O$-] in amine-cross linked epoxy whereas the latter to that of diphenyl groups in the backbone of epoxy network. Upon adding PHEMA-*g*-(PS-*b*-PCL)$_n$ to the epoxy, the α-transitions were observed to shift to lower temperature; the transition temperatures decreased with increasing the content of

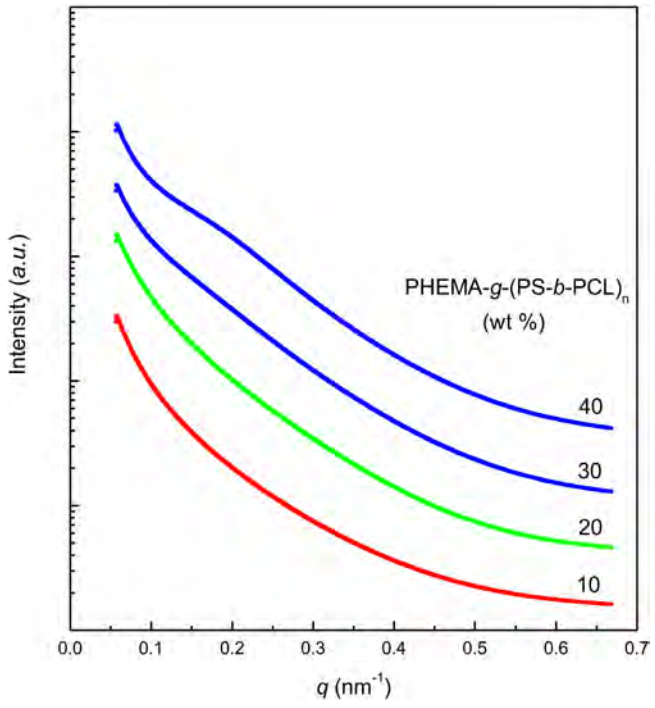

Fig. 7. SAXS profiles of the nanostructured thermosets containing PHEMA-*g*-(PS-*b*-PCL)$_n$ brush copolymer.

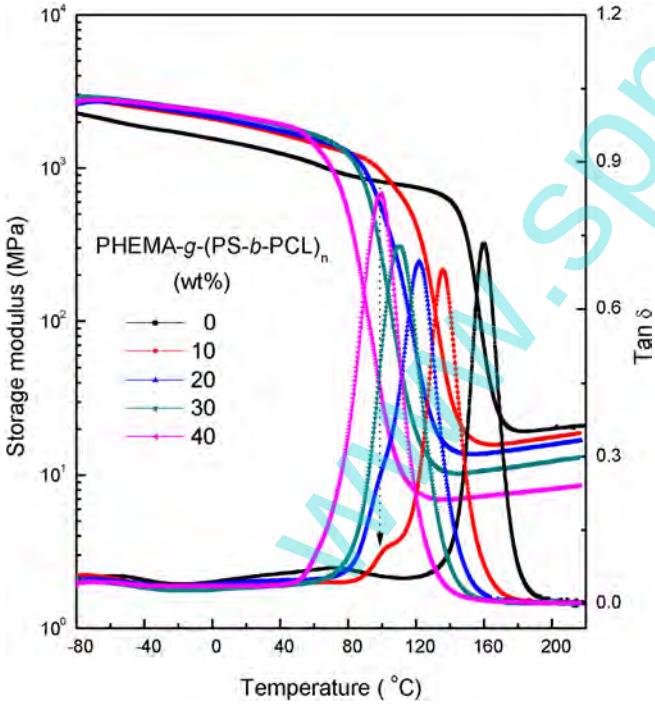

Fig. 8. DMTA curves of control epoxy and the binary blends of epoxy resin containing PHEMA-*g*-(PS-*b*-PCL)$_n$ brush copolymer. The content of copolymer is 10, 20, 30 and 40 *wt%*, respectively.

PHEMA-*g*-(PS-*b*-PCL)$_n$. The α-transition temperature was decreased to 99 °C while the content of PHEMA-*g*-(PS-*b*-PCL)$_n$ was 40 wt%. The decreased α-transition temperatures were attributable to the plasticization effect of the PCL blocks which possessed the T_g as low as −65 °C on epoxy matrices. In other word, the PCL subchains remained mixed with epoxy network at the segmental level. For the thermosets containing PHEMA-*g*-(PS-*b*-PCL)$_n$, there were additionally the major transitions at about 100 °C, the intensity of which increased with increasing the content of PHEMA-*g*-(PS-*b*-PCL)$_n$. These transitions are assignable to the PS microdomains. It is noted that the temperatures of transition for the PS microdomains remained almost invariant irrespective of the content of PHEMA-*g*-(PS-*b*-PCL)$_n$. While the contents of HEMA-*g*-(PS-*b*-PCL)$_n$ brush copolymer were 30 and 40 wt%, the α peaks of PS microdomains were overlapped with those of the α-transitions of epoxy matrices (See Fig. 8). The appearance of the major transitions assignable to PS and epoxy network indicates that the PS microdomains were indeed formed, *i.e.*, the epoxy thermosets containing PHEMA-*g*-(PS-*b*-PCL)$_n$ brush copolymer were microphase-separated.

3.3. Interpretation of nanofibrillar nanophases

By incorporating block copolymers into thermosets, the formation of nanophases in thermosetting polymers could follow self-assembly [52,53] or reaction-induced microphase separation (RIMPS) [54,55] mechanism. In self-assembly approach, the block copolymer is first self-organized into nanophases in the precursors of the thermosets; the pre-formed self-assembly nanophases were then fixed with the subsequent curing reaction. In RIMPS approach, all the copolymer blocks can be miscible with the precursors of the thermosets and no self-organized nanophases are formed before the curing reaction. The nanophases are not formed until the curing reaction occurs with the sufficiently high conversion. In the present case, a great number of PS-*b*-PCL diblocks were grafted onto a PHEMA chains and a cylindrical brush copolymer was obtained. It is of interest to investigate the formation mechanism of the fibrillar PS nanophases in epoxy thermosets. For this purpose, the mixtures of the precursors of epoxy (*i.e.*, DGEBA + MOCA) with the cylindrical brush copolymer bearing PS-*b*-PCL diblock copolymer side chains were subjected to small angle X-ray scattering (SAXS) after and before the curing reaction. Representatively shown in Fig. 9 are the SAXS profiles of the ternary mixture composed of DGEBA, MOCA and 10 wt% of PHEMA-*g*-(PS-*b*-PCL)$_n$. At room temperature (25 °C), the mixture displayed a broad and round scattering peak at $q = 0.28\ nm^{-1}$, corresponding to the principle spacing of $L = 22.4$ nm. The appearance of the broad and round scattering peak indicates that the mixture was microphase-separation at this temperature. The microphase separation could result from the self-assembly of the cylindrical molecular bush PHEMA-*g*-(PS-*b*-PCL)$_n$ in the precursors of epoxy (*viz.* DGEBA + MOCA) at room temperature. The microdomains formed in the mixture of the epoxy precursors and PHEMA-*g*-(PS-*b*-PCL)$_n$ could be the aggregates of PS blocks from a number of PHEMA-*g*-(PS-*b*-PCL)$_n$ brush copolymers. Upon heating the mixture to 150 °C, the scattering peak disappeared. This observation indicates that the mixture was homogenous at the elevated temperature, *i.e.*, the PS blocks were mixed with the epoxy precursors above the upper critical solution temperature (UCST) of the blends [56] (Scheme 3). After cured at 150 °C for 3 h, notably, the scattering intensity was significantly increased. The increase in scattering intensity indicates that the reaction-induced demixing occurred, which caused a compositional inhomogeneity. It is worth noticing that the scattering profile was no longer the broad and round peak as the mixture displayed before the curing reaction and at room temperature. The results of SAXS showed that the morphologies of the thermosets were quite different from those of the mixtures formed *via* self-assembly mechanism before curing reaction and at room temperature. The TEM showed that the reaction-induced demixing created the fibrillar PS nanophases.

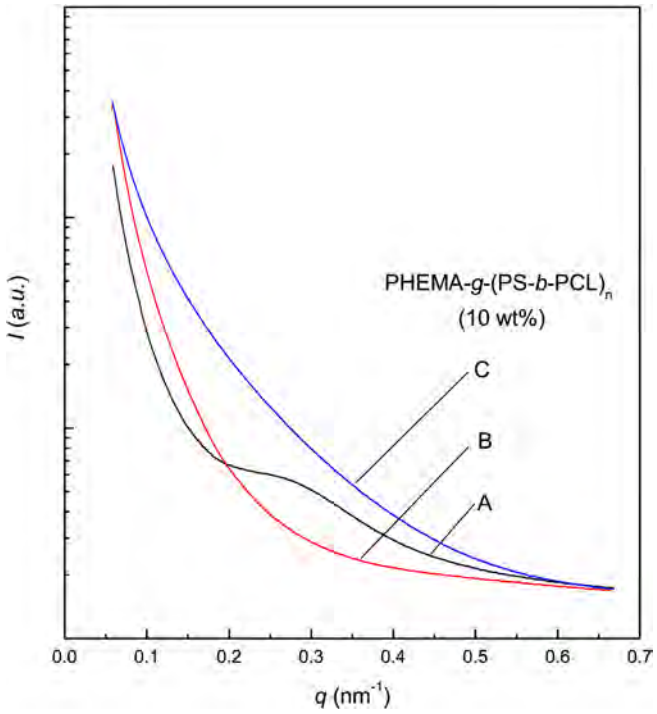

Fig. 9. SAXS profiles of the mixtures of epoxy precursors (*viz.* DGBBA + MOCA) with 10 *wt%* of PHEMA-*g*-(PS-*b*-PCL)$_n$ brush copolymer at: A) 25 °C, B) 150 °C and C) after cured at 150 °C for 3 h.

The formation of the fibrillar PS nanophases in the cured thermosets could be accounted for the restriction of the backbone chain (*viz.* PHEMA) on the demixing of PS blocks in epoxy thermoset. In the PHEMA-*g*-(PS-*b*-PCL)$_n$ brush copolymer, all the PS blocks were directly bonded onto a PHEMA backbone. At room temperature (before curing reaction), the PCL blocks were miscible with the precursors of epoxy whereas the PS blocks were microphase-separated out of the precursors owing to their immiscibility with the precursors of epoxy [49–51] as depicted in Scheme 3. Upon heating the mixtures to elevated temperature (*e.g.*, 150 °C), all the PS blocks became miscible with the precursors of epoxy, *i.e.*, all the PS and/or PCL subchains were solvated with the solvent (*viz.* the epoxy precursors). In the solutions, the cylindrical brush macromolecule took a conformation, in which the PHEMA backbone was stiffened with the dense PS-*b*-PCL grafts owing to the steric hindrance of the side chains [57,58]. In the reactive solutions, the cylindrical brush copolymer existed mainly in the disassembled and disentangled forms. As the curing reaction proceeded, the reaction-induced microphase separation of the PS blocks took place and thus the PS blocks began to segregate out of the solutions along with the PHEMA backbone. It is proposed that the reaction-induce demixing of PS subchains was undergone in a restricted manner due to: i) the extended cylindrical conformation of the brush-like copolymer and ii) its very high molecular weight (*viz.* M_n = 1,022,000Da). The extended cylindrical conformation resulted from the high steric crowding of the adjacent side chains which were densely bonded onto the backbone, *i.e.*, the cylindrical brush copolymer displayed the high rigidity of the backbone chain. This tendency hindered the intermolecular entanglement of the cylindrical brush macromolecules. As a consequence, a number of PHEMA-*g*-(PS-*b*-PCL)$_n$ brush copolymers were aggregated into the fibrillar nanodomains along the backbone in a parallel manner. The driving force to form the aggregation of the cylindrical brush copolymers was from the curing reaction, which gave rise to the decreased contribution of entropy to the mixing free energy due to the formation of the crosslinked networks. On the other hand, the extremely high molecular weight gave rise to the very low mobility of the giant molecule in the solutions; the more difficult the motion of the cylindrical brush copolymer the higher the degree of the curing reaction. The low mobility hindered a great number of cylindrical bush copolymers from aggregating (or fusing) into macroscopic domains. It should be pointed out that the presence of the miscible PCL blocks was critical. In the cylindrical brush copolymer, all the PCL subchains were connected to the PS chain ends and remained mixed with the epoxy network at the segmental scale and they behaved as the spacers between the PS subchains of the adjacent PHEMA-*g*-(PS-*b*-PCL)$_n$ brush copolymer. The miscibility of the PCL subchain with the epoxy network thus prevented a great number of cylindrical brush copolymer from forming the inter-molecular aggregation. In this case, the backbone of the cylindrical brush copolymer (*i.e.*, PHEMA) acted as a template to direct the alignment of PS blocks into the fibrillar microdomains and thus the fibrillar nanophases were formed in the cured thermosets.

4. Concluding remark

The PHEMA-*g*-(PS-*b*-PCL)$_n$ was successfully synthesized *via* the combination of atom transfer radical polymerization, the Huisgen 1,3-dipolar cycloaddition between azido and alkynyl groups and the ring-opening polymerization. The cylindrical brush copolymer was characterized by means of ^{1}H NMR, GPC, AFM and DSC. The cylindrical brush copolymer was microphase-separated in bulks as evidenced by DSC and AFM. The cylindrical brush copolymer was incorporated into epoxy to obtain the nanostructured thermosets. It was found that the reaction-induced microphase separation created the fibrillar PS nanophases in epoxy matrix as evidenced by TEM and SAXS. The formation of the PS nanofibers was interpreted in terms of the restriction of cylindrical architecture of the brush copolymer on the reaction-induced microphase separation of PS subchains in the cylindrical brush block copolymer. It is of interest to note that by the use of cylindrical brush copolymer bearing diblock side chains, the fibrillar nanophases of PS can be formed in the thermosets at a very low concentration of the additive (viz. bottlebrush copolymer). It is desirable to form percolation structures (*e.g.*, continuous nanophase) in the multicomponent polymers. It is expected that if these fibrillar nanophases result from some functional components such as electrical or thermal conductive polymers, the electrical, thermal conductive properties of the composite thermosets would be significantly improved. This is a new topic of investigation.

Acknowledgment

The financial supports from Natural Science Foundation of China (No. 51133003, 21274091 and 21304058) were gratefully acknowledged. The authors thank the Shanghai Synchrotron Radiation Facility for the support under the projects of Nos. 10sr0260 & 10sr0126. The authors thank Professor Daoyong Chen of Fudan University for the help to measure the polymer molecular weights by using the GPC apparatus equipped with a light scattering detector.

References

[1] S.S. Sheiko, B.S. Sumerlin, K. Matyjaszewski, Prog. Polym. Sci. 33 (2008) 759.
[2] H. Lee, J. Pietrasik, S.S. Sheiko, K. Matyjaszewski, Prog. Polym. Sci. 35 (2010) 24.
[3] J. Rzayev, ACS Macro Lett. 1 (2012) 1146.
[4] I. Park, D. Shirvanyants, A. Nese, K. Matyjaszewski, M. Rubinstein, S.S. Sheiko, J. Am. Chem. Soc. 132 (2010) 12487.

[5] K. Huang, J. Rzayev, J. Am. Chem. Soc. 131 (2009) 6880.
[6] K. Huang, D.P. Canterbury, J. Rzayev, Macromolecules 43 (2010) 6632.
[7] M. Zhang, A.H.E. Müller, J. Polym. Sci. Part A Polym. Chem. 43 (2005) 3461.
[8] Z. Li, J. Ma, N.S. Lee, K.L. Wooley, J. Am. Chem. Soc. 133 (2011) 1228.
[9] G. Sun, S. Cho, C. Clark, S.V. Verkhoturov, M.J. Eller, A. Li, A. Pavía-Jiménez, E.A. Schweikert, J.W. Thackeray, P. Trefonas, K.L. Wooley, J. Am. Chem. Soc. 135 (2013) 4203.
[10] C. Cheng, E. Khoshdel, K.L. Wooley, Macromolecules 40 (2007) 2289.
[11] Z. Li, J. Ma, C. Cheng, K. Zhang, K.L. Wooley, Macromolecules 43 (2010) 1182.
[12] J.A. Johnson, Y.Y. Lu, A.O. Burts, Y.-H. Lim, M.G. Finn, J.T. Koberstein, N.J. Turro, D.A. Tirrell, R.H. Grubbs, J. Am. Chem. Soc. 133 (2011) 559.
[13] M. Hu, Y. Xia, G.B. McKenna, J.A. Kornfield, R.H. Grubbs, Macromolecules 44 (2011) 6935.
[14] Y. Xia, B.D. Olsen, J.A. Kornfield, R.H. Grubbs, J. Am. Chem. Soc. 131 (2009) 18525.
[15] C. Cheng, E. Khoshdel, K.L. Wooley, Nano Lett. 6 (2006) 1741.
[16] W. Gu, J. Huh, S.W. Hong, B.R. Sveinbjornsson, C. Park, R.H. Grubbs, T.P. Russell, ACS Nano 7 (2013) 2551.
[17] C. Cheng, K. Qi, E. Khoshdel, K.L. Wooley, J. Am. Chem. Soc. 128 (2006) 6808.
[18] J. Bolton, T.S. Bailey, J. Rzayev, Nano Lett. 11 (2011) 998.
[19] C. Li, N. Gunari, K. Fischer, A. Janshoff, M. Schmidt, Angew. Chem. Int. Ed. 43 (2004) 1101.
[20] R. Djalali, S.-Y. Li, M. Schmidt, Macromolecules 35 (2002) 4282.
[21] M. Zhang, M. Drechsler, A.H.E. Müller, Chem. Mater 16 (2004) 537.
[22] M. Zhang, C. Estournes, W. Bietsch, A.H.E. Müller, Adv. Funct. Mater. 14 (2004) 871.
[23] C. Tang, B. Dufour, T. Kowalewski, K. Matyjaszewski, Macromolecules 40 (2007) 6199.
[24] Z. Li, K. Zhang, J. Ma, C. Cheng, K.L. Wooley, J. Polym. Sci. Part A Polym. Chem. 47 (2009) 5557.
[25] S. Jha, S. Dutta, N.B. Bowden, Macromolecules 37 (2004) 4365.
[26] Y. Xia, J.A. Kornfield, R.H. Grubbs, Macromolecules 42 (2009) 3761.
[27] H. Gao, K. Matyjaszewski, J. Am. Chem. Soc. 129 (2007) 6633.
[28] S.H. Lahasky, W.K. Serem, L. Guo, J.C. Garno, D. Zhang, Macromolecules 44 (2011) 9063.
[29] J. Sun, J. Hu, G. Liu, D. Xiao, G. He, R. Lu, J. Polym. Sci. Part A Polym. Chem. 49 (2011) 1282.
[30] H. Lee, W. Jakubowski, K. Matyjaszewski, S. Yu, S.S. Sheiko, Macromolecules 39 (2006) 4983.
[31] A. Nese, Y.C. Li, S. Averick, Y. Kwak, D. Konkolewicz, S.S. Sheiko, K. Matyjaszewski, ACS Macro Lett. 1 (2012) 227.
[32] J. Bolton, J. Rzayev, ACS Macro Lett. 1 (2012) 15.
[33] D. Zehm, A. Laschewsky, H. Liang, J.P. Rabe, Macromolecules 44 (2011) 9635.
[34] M. Zhang, T. Breiner, H. Mori, A.H.E. Müller, Polymer 44 (2003) 1449.
[35] J. Yuan, M. Drechsler, Y. Xu, M. Zhang, A.H.E. Müller, Polymer 49 (2008) 1547.
[36] H. Xu, D. Shirvanyants, K.L. Beers, K. Matyjaszewski, A.V. Dobrynin, M. Rubinstein, S.S. Sheiko, Phys. Rev. Lett. 94 (2005) 237801.
[37] M.O. Gallyamov, B. Tartsch, P. Mela, H. Boerner, K. Matyjaszewski, S. Sheiko, A. Khokhlovag, M. Möller, Phys. Chem. Chem. Phys. 9 (2007) 346.
[38] S.S. Sheiko, C. Frank, S. Adrian Randall, D. Shirvanyants, M. Rubinstein, L. Hyung-il, K. Matyjaszewski, Nature 440 (2006) 191.
[39] M.O. Gallyamov, B. Tartsch, A.R. Khokhlov, S.S. Sheiko, H.G. Berner, K. Matyjaszewski, M. Möller, Chem. Eur. J. 10 (2004) 4599.
[40] M.O. Gallyamov, B. Tartsch, P. Mela, I.I. Potemkin, S.S. Sheiko, H. BoeRner, K. Matyjaszewski, A.R. Khokhlov, M. Möller, J. Polym. Sci. Part B Polym. Phys. 45 (2007) 2368.
[41] C. Cheng, K. Qi, D.S. Germack, E. Khoshdel, K.L. Wooley, Adv. Mater. 19 (2007) 2830.
[42] G.M. Miyake, V.A. Piunova, R.A. Weitekamp, R.H. Grubbs, Angew. Chem. Int. Ed. 51 (2012) 11246.
[43] B.R. Sveinbjörnsson, R.A. Weitekamp, G.M. Miyake, Y. Xia, H.A. Atwater, R.H. Grubbs, Macromolecules 109 (2012) 14332.
[44] K. Huang, J. Rzayev, J. Am. Chem. Soc. 133 (2011) 16726.
[45] B.R. Sveinbjörnssona, R.A. Weitekamp, G.M. Miyake, Y. Xia, H.A. Atwater, R.H. Grubbs, Proc. Natl. Acad. Sci. U. S. A. 109 (2012) 14332.
[46] G.M. Miyake, R.A. Weitekamp, V.A. Piunova, R.H. Grubbs, J. Am. Chem. Soc. 134 (2012) 14249.
[47] W. Gu, J. Huh, S.W. Hong, B.R. Sveinbjornsson, C. Park, R.H. Grubbs, T.P. Russell, ACS Nano 7 (2013) 2551.
[48] S.W. Hong, W. Gu, J. Huh, B.R. Sveinbjornsson, G. Jeong, R.H. Grubbs, T.P. Russell, ACS Nano 7 (2013) 9684.
[49] M. Yin, S. Zheng, Macromol. Chem. Phys. 206 (2005) 929.
[50] Y. Ni, S. Zheng, Polymer 46 (2005) 5828.
[51] C. Sinturel, M. Vayer, R. Erre, H. Amenitsch, Macromolecules 40 (2007) 2532.
[52] M.A. Hillmyer, P.M. Lipic, D.A. Hajduk, K. Almdal, F.S. Bates, J. Am. Chem. Soc. 119 (1997) 2749.
[53] P.M. Lipic, F.S. Bates, M.A. Hillmyer, J. Am. Chem. Soc. 120 (1998) 8963.
[54] F. Meng, S. Zheng, W. Zhang, H. Li, Q. Liang, Macromolecules 39 (2006) 711.
[55] F. Meng, S. Zheng, H. Li, Q. Liang, T. Liu, Macromolecules 39 (2006) 5072.
[56] Z. Xu, S. Zheng, Macromolecules 40 (2007) 2548.
[57] S.S. Sheiko, S.A. Prokhorova, K.L. Beers, K. Matyjaszewski, I.I. Potemkin, A.R. Khokhlov, M. Möller, Macromolecules 34 (2001) 8354.
[58] M. Gerle, K. Fisher, S. Roos, A.H.E. Müller, M. Schmidt, Macromolecules 32 (1999) 2629.